Journal of Materials Chemistry

Cite this: DOI: 10.1039/c2jm32235h

www.rsc.org/materials

PAPER

Structural properties of solution processed $Ge_{23}Sb_7S_{70}$ glass materials

Maike Waldmann,[a] J. David Musgraves,[b] Kathleen Richardson[bc] and Craig B. Arnold*[a]

Received 10th April 2012, Accepted 21st July 2012
DOI: 10.1039/c2jm32235h

Solution-processing of chalcogenide glass materials has many benefits for the fabrication of photonic devices. We report on the structural properties of $Ge_{23}Sb_7S_{70}$ glass during solution-processing. The molecular and micro-structure of the bulk glass and the *n*-propylamine solution, as well as the spin-coated thin films and post-irradiated films are analyzed by Raman spectroscopy, scanning electron microscopy and energy dispersive X-ray spectroscopy. We find the vibrational spectral fingerprint of $Ge_4S_{10}^{4-}$-units in the amine solutions as well as in the spin-coated films, indicating a similar molecular structure of solutions and solution-processed films, which differs from the bulk glass. Moreover, the spin-coated films exhibit nanopores, and change their composition during irradiation such that sulfur escapes from the film while oxygen gets absorbed.

Introduction

Chalcogenide glass materials are important for a wide range of applications in photonic systems.[1–7] These glasses are transparent in the mid-infrared spectral range and, when shaped into waveguides, can provide devices for all-optical switching,[8] or for the development of integrated low-cost and easy-to-use trace gas sensors[9] which can be used in sensor networks to detect greenhouse gases. In particular, Ge–Sb–S systems have drawn attention for their photo-induced volume expansion and negative refractive index change, high nonlinear optical properties, as well as compositional tunability of various optical, chemical and structural properties.[10,11] This flexibility makes them especially attractive for integrated optical applications.

Conventionally, Ge–Sb–S glass films have been deposited either thermally, by sputtering, or by pulsed laser deposition.[12–14] However, solution-based processing offers a number of advantages. Dissolving the bulk chalcogenide glass first and then spin-coat the solution onto a substrate permits large area or thick film deposition, both of which are difficult to obtain through the previously mentioned deposition routes.[15–19] Another advantage of solution-based approaches is that the same solutions can be adopted for other deposition techniques such as mold casting[20,21] and ink jet printing.[22] Various chalcogenide materials dissolved in certain amines lead to homogeneous thin films that retain the optical, physical and chemical properties of the solute.[18,19] In particular, spin-coating of $Ge_{23}Sb_7S_{70}$ films with low surface roughness and controlled thickness has been demonstrated.[18] However, while solution-based approaches have a number of benefits for creating chalcogenide materials, little is known about the structural properties of $Ge_{23}Sb_7S_{70}$ solutions and the influence of the solvent and its subsequent removal on the resultant spin-coated glass films.

In this paper, we elaborate on the solution chemistry of $Ge_{23}Sb_7S_{70}$ glass in *n*-propylamine solutions and the molecular and micro-structure of spin-coated films in order to provide a better understanding about the dissolution mechanism, the solution processed material and fundamental knowledge for further investigation and application of $Ge_{23}Sb_7S_{70}$ thin films.

Materials and methods

Glass preparation

The $Ge_{23}Sb_7S_{70}$ bulk glass is prepared by a melt-quench process. A batch of 30 g of the high purity elements (Ge: Sigma-Aldrich 99.999%, Sb: Alfa-Aesar 99.999% and S: Cerac 99.999%) is weighed into a quartz ampoule under dry nitrogen gas atmosphere. The ampoule is sealed under vacuum, and heated for 16 h at 925 °C in a rocking furnace. The homogenized melt is then quenched in air and finally annealed for 16 h at 265 °C, 40 °C below the glass transition temperature of the resulting glass. Energy-dispersive X-ray spectroscopy (EDX) confirms the composition to be $Ge_{23}Sb_7S_{70}$.

Solution preparation

Solutions of $Ge_{23}Sb_7S_{70}$ are prepared by mixing between 0.5 g and 1.0 g finely ground bulk glass and 10 ml *n*-propylamine under nitrogen gas atmosphere in the glovebox in order to avoid chemical side-reactions with oxygen or water. The glovebox atmosphere exhibits levels of less than 1 ppm H_2O and O_2. The

[a]*Princeton Institute for the Science and Technology of Materials (PRISM), Princeton University, NJ 08544, USA. E-mail: cbarnold@princeton.edu; maikew@princeton.edu*
[b]*Center for Optical Materials Science and Engineering Technologies (COMSET), Clemson University, SC 29634, USA. E-mail: jdm047@clemson.edu*
[c]*School of Materials Science and Engineering, Clemson University, SC 29634, USA. E-mail: richar3@clemson.edu*

mixtures are stirred in sealed containers for at least 2 days. The resulting solutions are clear and have a green to yellow color; any precipitates that form in the process can be removed by filtration with a 0.1 μm PTFE syringe filter.

Film deposition and irradiation

Films are deposited by spin-coating onto glass microscope slides or silicon wafers under controlled atmosphere in the glovebox. Spin parameters of 1000 to 3000 rpm for 20 to 30 s lead to smooth films on the scale of 0.5–1 μm.[18] Immediately after spin-coating, the films are transferred to an oven and heated in a dry nitrogen atmosphere at 90 °C for 1 h, and then at 120 °C for 1 h under vacuum, to remove residual solvent. This temperature schedule was chosen to balance the need for solvent removal and the risk of film evaporation under vacuum that occurs at higher temperatures that approach the glass transition temperature. The composition of the spin-coated films is similar to the bulk glass, and the films are uniform in thickness and refractive index over the major area of the sample. Films are exposed to visible and UV light by irradiation with a broadband halogen lamp for an applied dose ranging from 0 to 2 kJ cm^{-2}.

Characterization

Raman spectroscopy is used to characterize the molecular structure of the bulk glass as well as the spin-coated glass thin films. Raman spectra were taken with a Bruker Senterra micro-Raman system (typical resolution of 2–3 cm^{-1}), in backscattering geometry at room temperature. The system consists of a holographic notch filter for Rayleigh rejection, a microscope equipped with 10×, 50× and 100× objectives, and a thermoelectrically cooled CCD detector. A 785 nm emission line from a diode laser source was used for excitation with incident power of around 10 mW. Raman spectroscopy of the solution was done using a Thermo Scientific DXR SmartRaman Spectrometer at 780 nm wavelength in a 180° configuration. Before measurement, the solution was filtered, filled into a measurement tube under nitrogen atmosphere and sealed. Scanning electron microscope (SEM) images were taken with a Quanta 200 FEG environmental SEM at 15 keV in high vacuum mode. The SEM is also equipped with an EDX system for the compositional analysis.

Results and discussion

Bulk glass structure

$Ge_{23}Sb_7S_{70}$ bulk glass is known to consist of [GeS_4] tetrahedra and [SbS_3] pyramids randomly linked either by shared sulfur atoms or by sulfur–sulfur bridges.[10] The Raman spectrum (Fig. 1a) also indicates the presence of molecular sulfur probably in the form of S_8 rings due to excess sulfur, since stoichiometrically, linked [GeS_4] and [SbS_3] units only account for 81% of the sulfur atoms when disregarding sulfur–sulfur bonds between units. Deconvolution of the glass main band (Fig. 1b) reveals the contributions of [SbS_3] pyramids, corner-shared (CS), and edge-shared (ES) [GeS_4] tetrahedra, CS meaning that two [GeS_4] tetrahedra share one sulfur atom while ES [GeS_4] tetrahedra share two sulfur atoms. Due to the more strained nature of ES

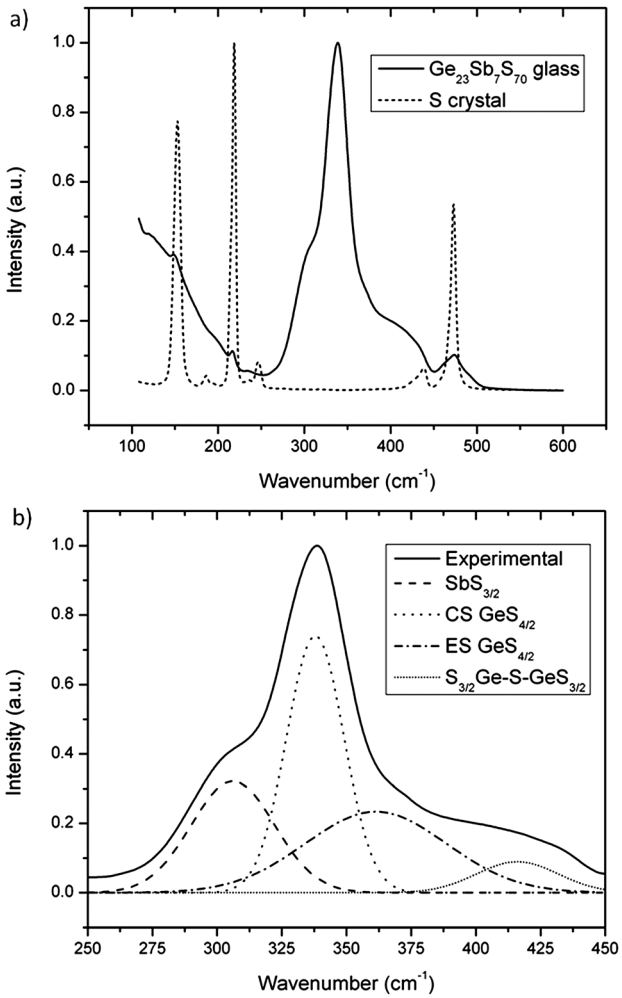

Fig. 1 (a) Comparison of the $Ge_{23}Sb_7S_{70}$ bulk glass Raman spectrum with that of elemental sulfur and (b) deconvolution of the main Raman band shows the glass structure (CS: corner-shared, ES: edge-shared GeS_4-tetrahedra).

tetrahedra, their contribution to the Raman signal is found at higher energies than the CS tetrahedra or the [SbS_3] pyramids.

Dissolution mechanism

Once dissolved in *n*-propylamine, $Ge_{23}Sb_7S_{70}$ exhibits a Raman spectrum similar to sodium tetrathiogermanate $Na_4Ge_4S_{10}$ and tetradodecylammonium tetrathiogermanate $(C_{12}H_{25}NH_3)_4Ge_4S_{10}$ crystals (Fig. 2),[23] indicating the formation of tetrathiogermanate $Ge_4S_{10}^{4-}$ ions in solution with their negative charge compensated for by *n*-propylammonium $C_3H_7NH_3^+$ ions, which have also been detected when dissolving the well-known arsenic sulfide (As_2S_3) glass in *n*-propylamine.[24] The adamantane-like tetrathiogermanate cluster, shown in the inset of Fig. 2, is formed by condensation of four [GeS_4] tetrahedra. This is possible because of the interaction of solvent and glass: the amine nitrogen acts as Lewis base and attacks the electropositive germanium or antimony which weakens or breaks germanium/antimony–sulfur bonds, facilitating reorientation of the [GeS_4] tetrahedra to form stable $Ge_4S_{10}^{4-}$ clusters. It is likely that these clusters exist as charged ions in amine solutions. Antimony sulfide species have

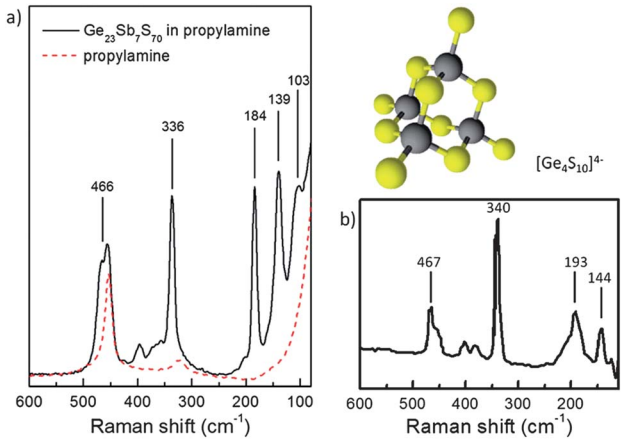

Fig. 2 Raman spectra of (a) dissolved $Ge_{23}Sb_7S_{70}$ and (b) $(C_{12}H_{25}NH_3)_4Ge_4S_{10}$ (ref. 23) agree.

been shown to exist in the presence of elemental sulfur in the oxidation state (+V) as $Sb_2S_6^{2-}$, as well as in mixed oxidation states (+V, +III) as in $Sb_2S_6^{4-}$.[25]

Molecular film structure

When depositing $Ge_{23}Sb_7S_{70}$ solution onto substrates by spin-coating, the formed thin films retain their molecular structure despite the major loss of solvent. The Raman spectra of spin-coated films therefore resemble the solution spectra more strongly than the bulk glass spectra (Fig. 3). The main differences between solution and film spectra are the absence of the solvent peak at 454 cm^{-1} (Fig. 3b) due to solvent evaporation during spincoating, the lower intensity and shifts of the main features to higher energies (194 and 345 cm^{-1}), the shift of the peak at 461 cm^{-1} to lower energies, and finally the appearance of a new peak at 555 cm^{-1}. The vibrational band at 345 cm^{-1} has been assigned to the symmetric breathing vibration of the $[Ge_4S_6]$ cage of the $Ge_4S_{10}^{4-}$ unit.[23] The shift to higher energies after deposition indicates a slightly more constrained geometry than in the free $Ge_4S_{10}^{4-}$ ions in solution which can be explained by the solid nature of the films. The vibrational band at 461 cm^{-1} is assigned to the symmetric stretching mode of the terminal [Ge–S^-] bonds. Its shift to lower energies after film deposition indicates a [Ge–S^-] bond weakening due to the formation of a more solid hydrogen bond between the terminal sulfur and adjacent propylammonium molecules. The origin of the newly formed band at 555 cm^{-1} is so far unknown.

Microscopic film structure

The microscopic structure of spin-coated $Ge_{23}Sb_7S_{70}$ thin films (cross section of a cleaved film in Fig. 4a) shows nanopores which have also been found in $M_x(Ge_4S_{10})_y$ compounds with amine-based surfactants added,[23,26] although the pores found here have comparatively large diameters of approximately 200 nm. The material network is formed by $[Ge_4S_{10}]$ tetrahedra interlinked by either sulfur chains or $[SbS_3]$ units. We hypothesize that the porous cavities are formed by micelle-like solvent accumulation during spin-coating. We noticed that pores at the surface appear to be closed whereas those at a freshly cleaved edge appear to be open. The pores at the surface are closed due to evaporation and

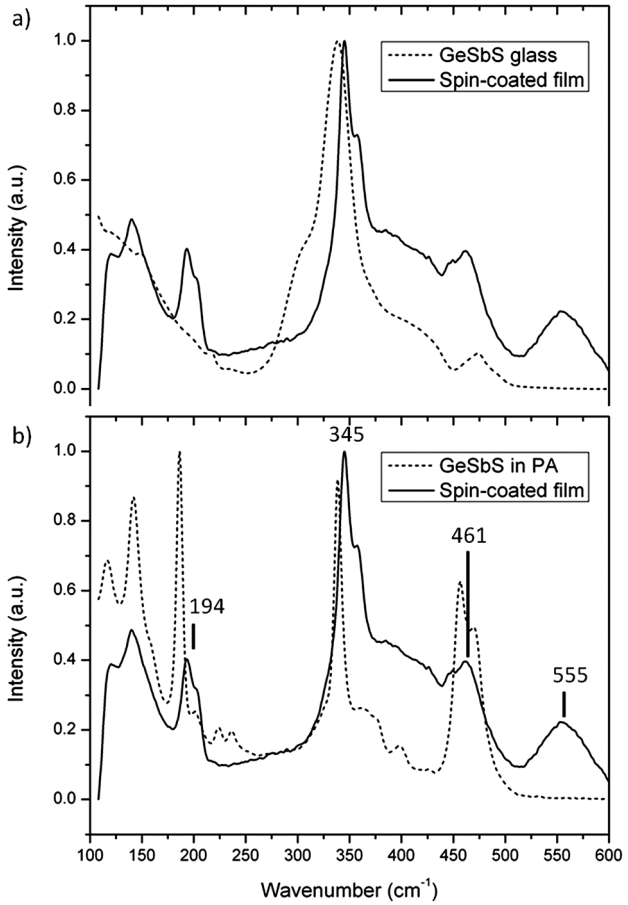

Fig. 3 Raman spectrum of spin-coated film is more similar to solution than to bulk glass.

reconfiguration of the glass network. We believe that once these pores close, additional solvent is trapped and cannot escape. Upon cleaving, the solvent is able to escape, leaving behind open pores at the cleaved edges.

Irradiation effects

Shining light from a broadband light source affects the chemical properties of the films. Sulfur is released from the film, forming sulfur patches on the film surface (Fig. 4c). The Raman spectrum of the irradiated films shows the distinct pattern of S_8 rings with bands at 150, 218 and 471 cm^{-1} (Fig. 5). But the formation of elemental sulfur is not the only observed compositional change. The total sulfur content decreases while at the same time oxygen enters the film, and an increased oxygen-content following irradiation can be found in the films by means of EDX analysis (Fig. 6). The oxygen content of the unirradiated films is due to their transport and fracture in an air environment, and can be viewed as an instrument artifact. Nonetheless, there is a clear reduction in the Sb content of the deposited films, which supports the changes in the Raman spectra shown in Fig. 3, and indicates that some of the Sb is removed as a precipitate when the solution is filtered before deposition. This reduction in the Ge/Sb ratio during solution processing is opposite the behaviour exhibited by thermally evaporated films of the same composition, which show an increase in Ge/Sb due to preferential volatilization of the glass

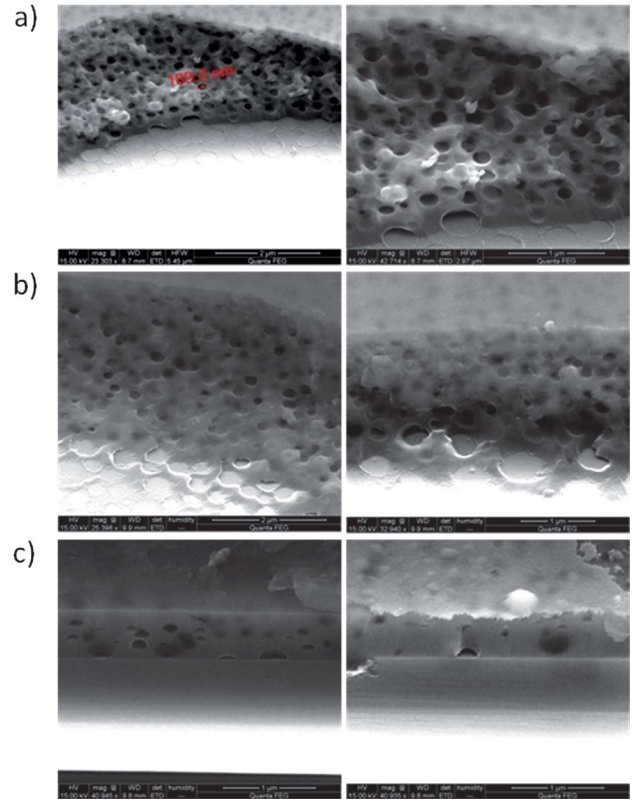

Fig. 4 (a) Spin-coated $Ge_{23}Sb_7S_{70}$ thin films are nanoporous; pores are closed on the surface. (b) Irradiated $Ge_{23}Sb_7S_{70}$ thin films exhibit less pores, many of which are closed, especially closer to the surface. (c) Films which have been baked first (at 120 °C) and irradiated afterwards still exhibit pores, as well as sulfur patches on the surface.

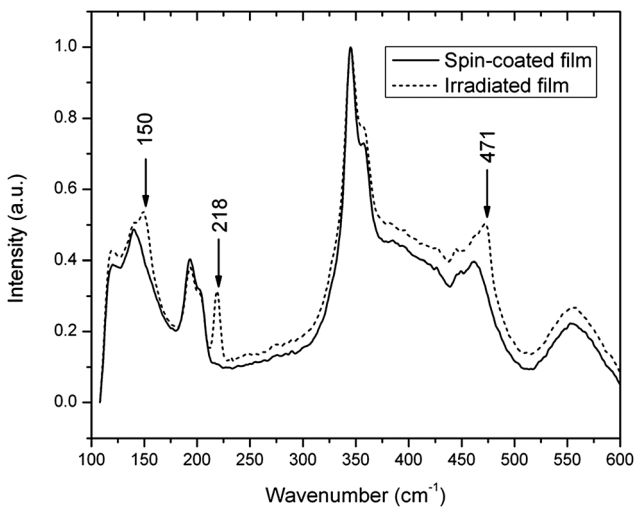

Fig. 5 Raman spectrum of irradiated $Ge_{23}Sb_7S_{70}$ film indicates formation of sulfur chains.

components during deposition.[27] After irradiation for an extended period of time, germanium oxide crystals can be found on the film surface (with a Ge : O ratio of 1 : 2.5). Despite these major compositional changes the pre-exposure micro-structure remains basically unchanged after irradiation (Fig. 4b and c) apart from a qualitative decrease of pore size and number. The

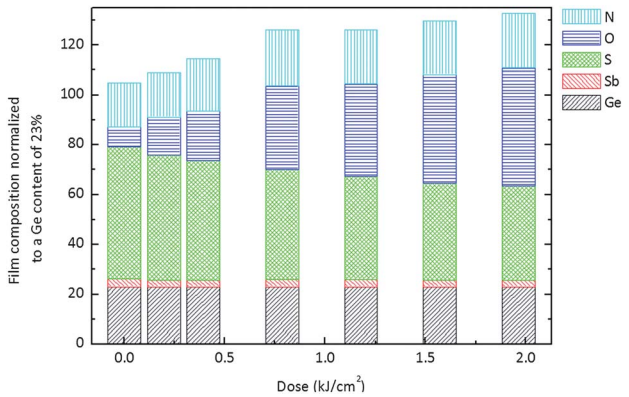

Fig. 6 Sulfur content of spin-coated $Ge_{23}Sb_7S_{70}$ thin film decreases as oxygen content increases with irradition dose (EDX measurements). Contents are relative and normalized to the starting Ge content of 23%. Nitrogen represents constant residual solvent content.

changes will nonetheless have an important effect on the optical properties of these films.[10]

Conclusion

We have investigated the structural changes during solution-processing of $Ge_{23}Sb_7S_{70}$ glass, starting from the molecular structure of the bulk material, looking at the dissolved species in the *n*-propylamine solution, and comparing the latter to the spin-coated films. Dissolved $Ge_{23}Sb_7S_{70}$ glass exists as $Ge_4S_{10}^{4-}$ clusters and likely $Sb_2S_6^{2-}$ and $Sb_2S_6^{4-}$ in *n*-propylamine solution, charge compensated by propylammonium ions. Spin-coating leads to smooth surfaced, yet nanoporous thin films which retain the molecular structure of the solution rather than the original bulk material. We have also defined compositional and mechanistic changes when the films are irradiated with a broadband light source. Sulfur escapes the film and forms elemental sulfur patches on the film surface. Since the original composition stoichiometrically possesses excess sulfur, we explain this by suggesting that the light causes the breaking of homopolar bonds (Ge–Ge) to form heteropolar bonds (similar to Ge–Se bonds as in[28]), thus decreasing the overall density and releasing elemental sulfur. This leads to a better interlinked network with decreased pore size. The elemental sulfur is then removed by photo-enhanced oxidation. Based on this work we gain a better understanding of the solution chemistry in this important material system, leading to improved control over the chemical and physical properties for the optimization of these materials.

Acknowledgements

This work was supported by National Science Foundation (NSF) grant EEC-0540832 through the Center of Mid-Infrared Technologies for Health and the Environment (MIRTHE). M.W. acknowledges the German Academic Exchange Service (DAAD) for generous support within the postdoctoral fellowship program. Funding to the Clemson researchers has been provided in part, by the US Department of Energy [Contract # DE- NA000421], NNSA/DNN R&D. This paper has been prepared as an account of work partially supported by an agency

Notes and references

1 A. Ganjoo, H. Jain, C. Yu, R. Song, J. Ryan, J. Irudayaraj, Y. Ding and C. Pantano, *J. Non-Cryst. Solids*, 2006, **352**(6–7), 584–588. New Functionality of Glasses – Proceedings of the 17th University Conference on Glass Science.
2 V. Ta'eed, N. J. Baker, L. Fu, K. Finsterbusch, M. R. E. Lamont, D. J. Moss, H. C. Nguyen, B. J. Eggleton, D.-Y. Choi, S. Madden and B. Luther-Davies, *Opt. Express*, 2007, **15**(15), 9205–9221.
3 F. Luan, M. D. Pelusi, M. R. E. Lamont, D.-Y. Choi, S. Madden, B. Luther-Davies and B. J. Eggleton, *Opt. Express*, 2009, **17**(5), 3514–3520.
4 B. J. Eggleton, B. Luther-Davies and K. Richardson, *Nat. Photonics*, 2011, **5**, 141–148.
5 A. B. Seddon, *J. Non-Cryst. Solids*, 1995, **184**, 44–50. Non-oxide Glasses.
6 A. Zakery and S. R. Elliott, *J. Non-Cryst. Solids*, 2003, **330**(1–3), 1–12.
7 N. Carlie, J. D. Musgraves, B. Zdyrko, I. Luzinov, J. Hu, V. Singh, A. Agarwal, L. C. Kimerling, A. Canciamilla, F. Morichetti, A. Melloni and K. Richardson, *Opt. Express*, 2010, **18**(25), 26728–26743.
8 M. Galili, J. Xu, H. C. Mulvad, L. K. Oxenløwe, A. T. Clausen, P. Jeppesen, B. Luther-Davies, S. Madden, A. Rode, D.-Y. Choi, M. Pelusi, F. Luan and B. J. Eggleton, *Opt. Express*, 2009, **17**(4), 2182–2187.
9 C. Tsay, F. Toor, C. F. Gmachl and C. B. Arnold, *Opt. Lett.*, 2010, **35**(20), 3324–3326.
10 L. Petit, N. Carlie, F. Adamietz, M. Couzi, V. Rodriguez and K. Richardson, *Mater. Chem. Phys.*, 2006, **97**(1), 64–70.
11 L. Petit, N. Carlie, A. Humeau, G. Boudebs, H. Jain, A. Miller and K. Richardson, *Mater. Res. Bull.*, 2007, **42**(12), 2107–2116.
12 K. Tanaka, Y. Kasanuki and A. Odajima, *Thin Solid Films*, 1984, **117**(4), 251–260.
13 V. Balan, C. Vigreux and A. Pradel, *J. Optoelectron. Adv. Mater.*, 2004, **6**, 875–882.
14 K. E. Youden, T. Grevatt, R. W. Eason, H. N. Rutt, R. S. Deol and G. Wylangowski, *Appl. Phys. Lett.*, 1993, **63**(12), 1601–1603.
15 J. Santiago, M. Sano, M. Hamman and N. Chen, *Thin Solid Films*, 1987, **147**(3), 275–284.
16 S. Shtutina, M. Klebanov, V. Lyubin, S. Rosenwaks and V. Volterra, *Thin Solid Films*, 1995, **261**(1–2), 263–265.
17 T. Kohoutek, T. Wagner, M. Frumar, A. Chrissanthopoulos, O. Kostadinova and S. N. Yannopoulos, *J. Appl. Phys.*, 2008, **103**(6), 063511.
18 S. Song, N. Carlie, J. Boudies, L. Petit, K. Richardson and C. B. Arnold, *J. Non-Cryst. Solids*, 2009, **355**(45–47), 2272–2278.
19 S. Song, J. Dua and C. B. Arnold, *Opt. Express*, 2010, **18**(6), 5472–5480.
20 C. Tsay, Y. Zha and C. B. Arnold, *Opt. Express*, 2010, **18**(25), 26744–26753.
21 C. Tsay, E. Mujagic, C. K. Madsen, C. F. Gmachl and C. B. Arnold, *Opt. Express*, 2010, **18**(15), 15523–15530.
22 E. A. Sanchez, M. Waldmann and C. B. Arnold, *Appl. Opt.*, 2011, **50**(14), 1974–1978.
23 K. K. Rangan and M. G. Kanatzidis, *Inorg. Chim. Acta*, 2004, **357**(13), 4036–4044.
24 G. C. Chern and I. Lauks, *J. Appl. Phys.*, 1983, **54**(5), 2701–2705.
25 G. R. Helz, M. S. Valerio and N. E. Capps, *Environ. Sci. Technol.*, 2002, **36**(5), 943–948. PMID: 11918022.
26 M. Wachhold, K. K. Rangan, M. Lei, M. Thorpe, S. J. Billinge, V. Petkov, J. Heising and M. G. Kanatzidis, *J. Solid State Chem.*, 2000, **152**(1), 21–36.
27 J. D. Musgraves, N. Carlie, J. Hu, L. Petit, A. Agarwal, L. C. Kimerling and K. A. Richardson, *Acta Mater.*, 2011, **59**(12), 5032–5039.
28 G. Yang, H. Jain, A. Ganjoo, D. Zhao, Y. Xu, H. Zeng and G. Chen, *Opt. Express*, 2008, **16**(14), 10565–10571.